JMEPEG (2012) 21:2675–2679
DOI: 10.1007/s11665-012-0268-2

1059-9495/$19.00

Study of Thermal Scanning Rates on Transformations of Ti-19Nb-9Zr (at.%) by Means of Differential Scanning Calorimetry Analysis

L.W. Ma, H.S. Cheng, C.W. Cao, and C.Y. Chung

(Submitted February 20, 2012; in revised form May 7, 2012)

Differential scanning calorimetry (DSC) thermal analysis is a well-accepted technique used to measure the transformation temperatures of shape memory alloy and its thermoelastic transformation energies. In this study, both forward and reverse transformation temperatures of a nickel-free Ti-19Nb-9Zr (at.%) SMA were investigated using DSC technique with different cooling and heating scanning rates in a range of 10 to 100 °C/min. The results showed that the transformation temperature intervals vary substantially with respect to the thermal scanning rates. It is found that the martensitic start (M_s) temperature decreases with decreasing the cooling rates. The optimal scanning rate was found to be 40 °C/min for obtaining the maximum thermoelastic transformation energies stored between the forward and the reverse martensitic transformations. It is believed that the thermoelastic transformation energy increases with the increase in the volume fraction of martensite. Based on these measurements, these thermoelastic transformation energies between the forward and the reverse martensitic transformations were estimated to be ~21 and ~27 J/g, respectively. The appropriate selection of scanning rate for SMA analysis will be discussed.

Keywords differential scanning calorimetry (DSC) thermal analysis, shape memory alloy, thermal scanning rate, Ti-Nb-Zr alloy

1. Introduction

Nickel-titanium (NiTi) shape memory alloys (SMA) have been widely used in biomedical application owing to its superior shape memory property, superelasticity, and corrosion resistance. However, Ni ions released from these alloys have been recently reported to cause detrimental effect to humans, particularly in Ni hypersensitive patients resulting in strong allergic response (Ref 1). In order to overcome such problem, Ni-free Ti-based SMAs are considered more because they are non-toxic and biocompatible (Ref 2-4).

Baker (Ref 5) reported that a cold rolled Ti-35 wt.% Niobium (Nb) binary alloy exhibits shape memory effect in 1971. Kim et al. (Ref 6) performed a series of investigation on the mechanical properties and morphologies of Ti-Nb binary alloys, which were fabricated by an arc melting method. Stable shape memory behaviour and superelasticity were observed in Ti-(22-25)Nb (at.%) and Ti-(25.5-27)Nb (at.%) alloys, respectively. They concluded that solid solution-treated Ti-(25-27)Nb (at.%) possess the highest recovered strain of 3%. More recently, other researchers further investigated the properties of Ti-Nb SMA by adding ternary elements, including molybdenum (Mo), palladium (Pd), tin (Sn), zirconium (Zr), etc. Kim et al. (Ref 7) studied the shape memory characteristics of arc-melted Ti-22Nb-(2-8)Zr (at.%) alloys by means of tensile tests and x-ray diffraction (XRD) measurement. The martensitic transformation temperature was found to decrease by 38 K with 1 at.% increase of Zr content in thermomechanical cyclic test. The maximum recoverable thermoelastic strain of 4.3% was also obtained in the Ti-22Nb-4Zr (at.%) alloy.

Recently, Chang and Wu (Ref 8) had investigated the effect of cooling rate on transformation temperature measurements of NiTi using differential scanning calorimetry (DSC) thermal analysis because of DSC is effective in measuring transformation temperature intervals and thermoelastic transformation energies of the SMA (Ref 9). They found that the transformation temperature of specimen with greater mass increases more rapidly at slower cooling rates. However, the specimen size effect would become negligible when the cooling rate was close to zero. The objective of this study is to investigate the effect of both cooling and heating rates on transformation temperatures determined for Ni-free Ti-19Nb-9Zr (at.%) SMA. The study employs a combination of the DSC and XRD analysis. To this end, the microstructure of the alloy will be examined by transmission electron microscopy (TEM). Different scanning rates, ranging from 10 to 100 °C/min, were used to determine the transformation temperatures. XRD was used to examine the crystallographic structure of the alloy.

2. Experimental Procedure

Ti19Nb9Zr (at.%) ingot was fabricated from pure Ti(99.9% purity), Nb(99.8% purity), and Zr(99.8% purity) cubes using a

This article is an invited paper selected from presentations at the International Conference on Shape Memory and Superelastic Technologies 2011, held November 6-9, 2011, in Hong Kong, China, and has been expanded from the original presentation.

L.W. Ma, H.S. Cheng, C.W. Cao, and **C.Y. Chung**, Department of Physics and Materials Science, City University of Hong Kong, 83 Tat Chee Avenue, Kowloon Tong, Hong Kong. Contact e-mails: robin.ma@cityu.edu.hk and appchung@cityu.edu.hk.

vacuum arc melting furnace. The ingot was cold-rolled to a 90% reduction. The as-rolled specimens were initially cut using an electrical discharge machine, and then were annealed at a temperature of 700 °C for 30 min. The purpose of this annealing is to ensure that the deformed microstructure is thoroughly recrystallized. The phase transformation temperatures of the annealed specimen were then characterized using the Perkin Elmer DSC 7 thermal analyzer. The specimen weight for the DSC was ~50 mg with a dimension of about $4.5 \times 4.5 \times 0.9$ mm, while the heating/cooling rates varied from ±10 to ±100 °C/min. Hereafter, the annealed specimens are named according to their different heating/cooling rates. For example, the specimen heated/cooled with a rate of 10 °C/min was denoted as SR10. Therefore, six different specimens in total were used in this study and they are SR10, SR20, SR30, SR40, SR50, and SR100. The constituent phases of all SR specimens were investigated using XRD analysis with Cu Kα source (λ = 1.5406 Å) in 2θ ranges between 30° and 80°. The microstructure was investigated using a JSM 820 scanning electron microscope and a CM20 TEM. The SEM specimens were etched by the solution of HF, HNO_3, and H_2O with a composition in proportion of 2:1:17 (volume ratio). TEM specimens were prepared by electrochemical polishing using an electrolyte of 6% perchloric acid + 35% butanol + 59% methanol at −10 °C. The Vickers microhardness (HV) values of all specimens were measured by applying a load of 1000 g for 10 s and taking an average of 10 individual readings using a Martsuzawa MXT-CX7 Digital Microhardness Tester.

3. Results and Discussion

Figure 1(a) and (b) shows the heating and the cooling DSC curves, respectively, of the annealed specimens subjected with different rates varied from 10 to 100 °C/min (SR10-SR100). The transformation temperatures and energies of all specimens measured from the DSC curves are listed in Table 1.

In Fig. 1, it can be seen that all DSC curves are highly associated with the heating/cooling rates during the test. The M_s temperatures of the specimens ranged from 269 to 303 °C and was found to decrease with increasing the cooling/scanning rate. It is also noted that both forward and reverse martensitic transformation peaks become sharper when increasing the heating/cooling rates from 10 to 40 °C/min. Thus, increasing the heating/cooling rates after heat treatment is more favorable to the martensitic transformation. Also, the highest thermoelastic transformation energies stored between the forward and the reverse martensitic transformations were found to be 21 and 27 J/g, respectively, with the heating/cooling rate of 40 °C/min. It is suggested that the heating/cooling rate of 40 °C/min is the optimal scanning rate for the formation of martensite in the proposed alloy because of the highest thermoelastic transformation energy (21 J/g) was obtained according to the DSC curves in Fig. 1(b). However, starting from a cooling rate of 50 °C/min, a profound decrease in the M_s temperature and thermoelastic transformation energies stored between the transformations were observed. It is possibly due to the formation of athermal ω phase during the fast cooling rate between 50 and 100 °C/min. It has been well documented (Ref 10) that the arc-melted TiNb-based SMA consisted of the athermal ω phase and β phase is expected to hinder the partial martensitic transformation and leads to a drop in the M_s temperature. Accordingly, the athermal ω phase can effectively stabilize the parent β phase, thus suppressing the martensitic transformation.

The specimens were examined by XRD after the DSC analysis. Figure 2 shows the XRD profiles of the (a) as-rolled, (b) SR10, (c) SR40, and (d) SR100 specimens.

Stress-induced martensites and β phase were observed in the as-rolled specimen. It is noted that the diffraction peaks of the as-rolled specimen were broaden due to the accumulation of residual stress and the distortion of the lattice after cold rolling. In contrast, comparatively sharper diffraction peaks indicating α″ and β phase were observed for specimens after heat treatment, suggesting grains orientation and/or size might be changed during re-crystallization of the heat-treated specimens.

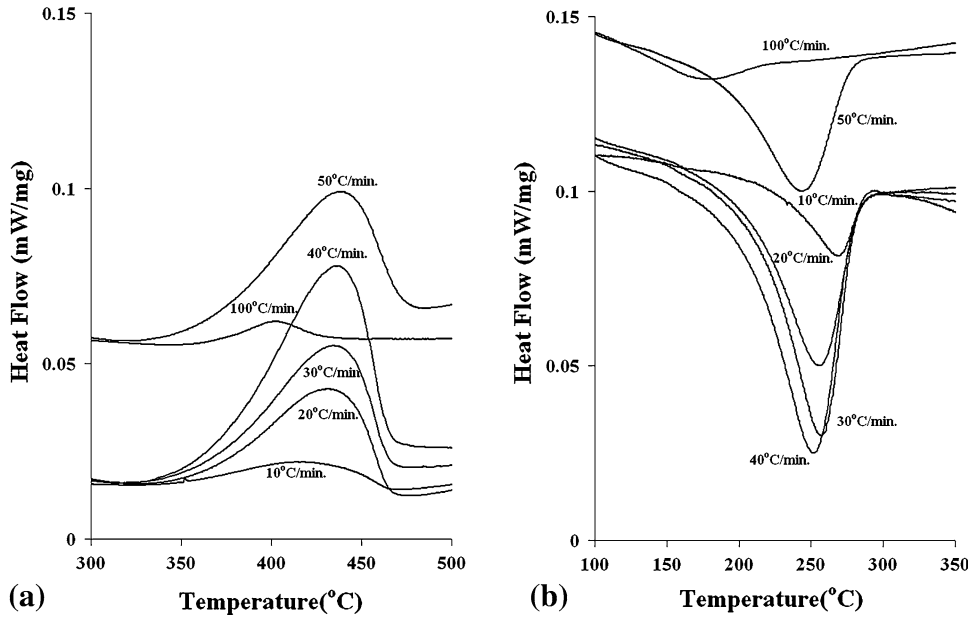

Fig. 1 (a) The heating and (b) the cooling DSC curves of the annealed specimens subjected to different rates varied from 10 to 100 °C/min (SR10-SR100)

Table 1 The transformation temperatures and energies of all specimens measured from the DSC curves

	M_f, °C	M_s, °C	E_M, J/g	A_f, °C	A_s, °C	E_A, J/g
SR10	184	303	9.3	471	343	12.7
SR20	144	298	13.4	470	344	13.2
SR30	143	297	19	471	331	25.9
SR40	133	293	21	473	334	27.0
SR50	147	277	16.8	475	333	24.5
SR100	220	269	3.9	434	352	7.1

M_f, Martensite finish temperature; M_s, martensite start temperature; A_f, austenite finish temperature; A_s, martensite start temperature; E_M, Thermoelastic transformation energy stored in the martensitic transformation; E_A, Thermoelastic transformation energy stored in the austenitic transformation

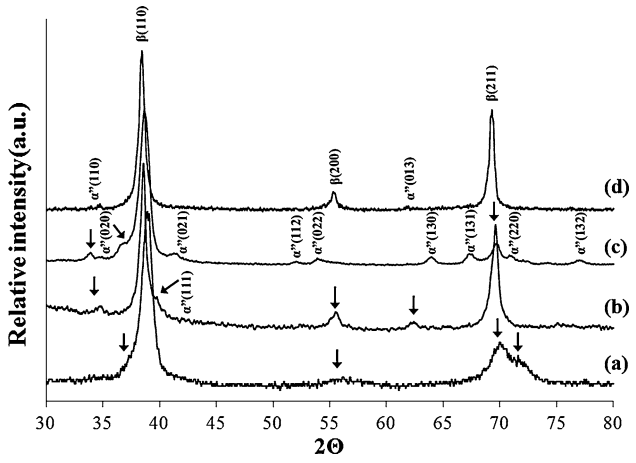

Fig. 2 XRD profiles of the (a) as-rolled, (b) SR10, (c) SR40, and (d) SR100 specimens

On the other hand, a relative large amount of α″ martensite was found in the SR40 specimen while the β phase was largely retained in the SR10 and SR100 specimens. However, the peak corresponding to ω phase was not detected by the XRD measurement due to a very small amount in volume fraction in the SR100 specimen. Hence, the TEM was used to confirm the presence of ω phase in the SR100 specimen that will be discussed later. It should be noted again that the heating/cooling rate of 40 °C/min is the optimal scanning rate for the formation of martensite (SR40) in the proposed alloy. This is consistent with a SEM image of the morphology of martensites shown in Fig. 3(a). A large amount of fine needle-like traces of martensite within the equiaxed β-phase matrix can be observed in the SR40 specimen. Also, the grain structures with a dimension of approximately 60 μm were observed. Figure 3(b) is a higher magnification SEM image of the same sample shown in (a). In contrast, a very small amount of martensite, marked by an arrow, was found in the SR100 specimen (Fig. 3c).

Figure 4 shows the dark-field TEM image of athermal ω phase in the SR100 specimen ($[113]_\beta$ SAD pattern was also inserted). This dark-field TEM image was formed using the spot of athermal ω phase in the diffraction patterns marked by a circle. Fine athermal ω particles with dimensions of approximately 20 nm were observed.

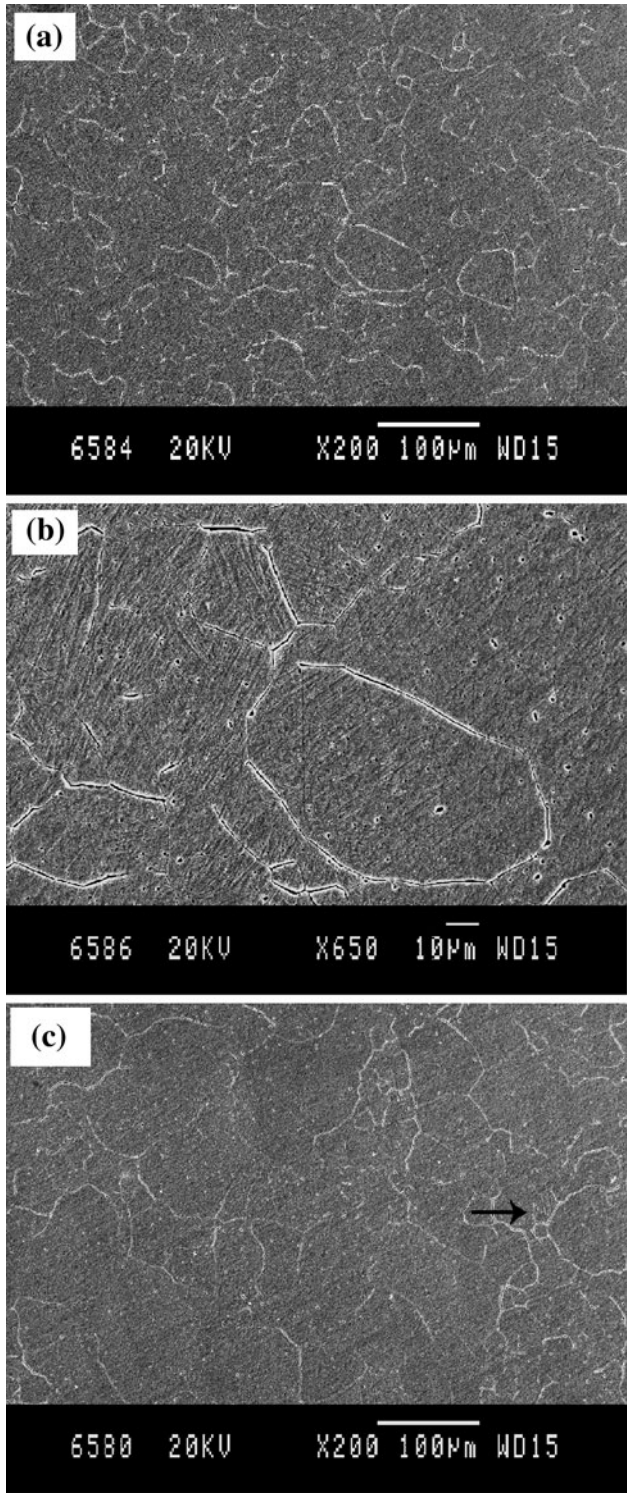

Fig. 3 SEM image of the morphology of martensites in (a) SR40 specimen, (b) SR40 specimen at higher magnification, and (c) SR100 specimen

Figure 5 shows the change in hardness values of all specimens. Surprisingly, the variation of hardness values was found to be highly associated with the thermoelastic transformation energies stored during the forward martensitic transformation as listed in Table 1.

The hardness values decreased starting of a cooling rate from 10 to 40 °C/min then increased with further increasing of

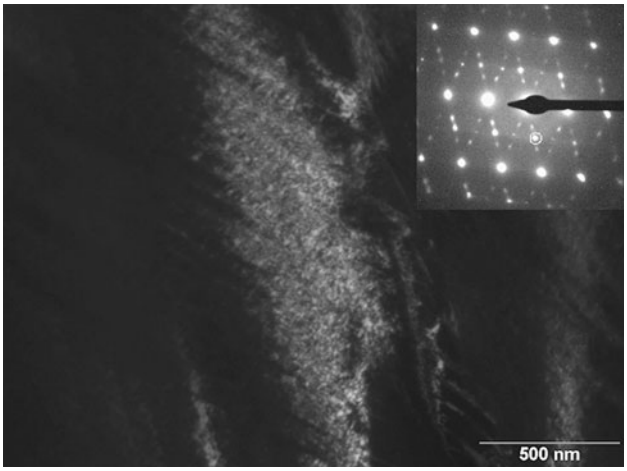

Fig. 4 Dark-field TEM image of athermal ω phase in the SR100 specimen ([113]$_\beta$ SAD pattern was also inserted)

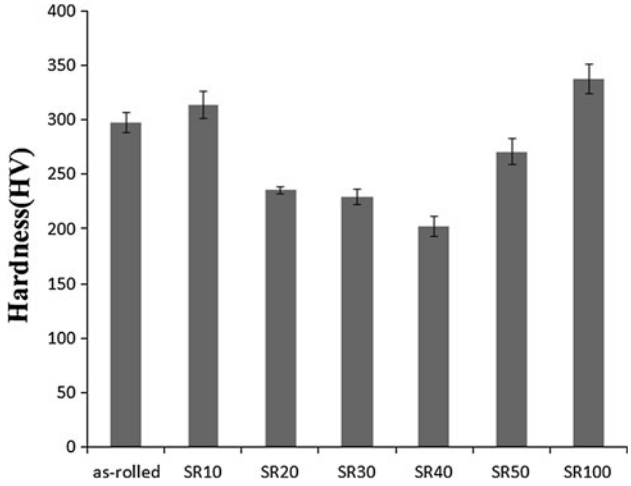

Fig. 5 The change in hardness values of all specimens

the cooling rate from 50 to 100 °C/min. The decrease in hardness of the specimens was probably due to increase in amount of α″ martensites, since more volume fraction of α″ martensite was found in SR40 specimen (Fig. 3b). The α″ phase-dominated SR40 specimen had the lowest Vicker's hardness of 203HV. For cooling rate higher than 40 °C/min, the hardness increased again gradually. The increase in hardness value again is possibly due to the formation of athermal ω phase (Fig. 4) and the decrease in volume fraction of α″ martensite (Fig. 3c). It was documented that the athermal ω phase suppresses the β → α″ martensitic transformation and causes profound effect on the mechanical properties of the alloy (Ref 10). The effect of athermal ω phase on the hardness of Ti-Mo-Fe alloy was also studied by Lin et al. (Ref 11). They suggested that increasing the amount of Fe content leads to increasing in the amount of athermal ω phase, a strong hardening effect was observed in the alloy with larger quantity of athermal ω phase. As shown in the present results, the amount of athermal ω phase was also sensitive to cooling rate after heat treatment.

From an engineering point of view, the formation of both athermal and isothermal ω phase should be avoided as it may cause brittleness to the alloy. Many researchers intended to change the composition of the alloy preventing ω-induced brittleness (Ref 12). However, changing the composition of the alloy may also cause a change in the martensitic transformation temperature which may also affect the superelasticity or shape memory effect of the alloy. In the present results, selecting different heating/cooling rates (scanning rate) using the DSC analysis after heat treatment can be an alternative method suppressing the formation of athermal ω phase while not changing the shape memory effect of the alloy. Also, it is believed that the thermomechanical properties of the proposed alloy could be improved using some proper thermal treatments followed by selecting the correct heating/cooling rate, which will be further investigated.

4. Conclusions

The study of thermal scanning rates on transformations of Ti-19Nb-9Zr (at.%) was successfully examined by means of DSC analysis. The M_s temperatures of the specimens ranged from 269 to 303 °C were found to decrease linearly with increasing the cooling rate. The biggest thermoelastic transformation energies stored between the forward and the reverse martensitic transformations were found to be 14 and 27 J/g, respectively, with the heating/cooling rate of 40 °C/min. It is believed that the heating/cooling rate of 40 °C/min is the optimal scanning rate for the formation of martensite in the proposed alloy. However, starting from a cooling rate of 50 °C/min, a profound decrease in the M_s temperature due to the formation of athermal ω phase during the fast cooling rate between 50 and 100 °C/min was observed. A relative large amount of α″ martensite was found in the SR40 specimen while the β phase was largely retained in the SR10 and SR100 specimens. A large amount of fine needle-like traces of martensite with the presence of β-phase matrix can be observed in the SR40 specimen while fine athermal ω particles with dimensions of approximately 20 nm were observed in the SR100 specimen. Finally, the hardness values decreased starting of a cooling rate from 10 to 40 °C/min then increased with further increasing of the cooling rate from 50 to 100 °C/min. The SR40 specimen was found to have the lowest Vicker's hardness value of 203HV.

Acknowledgment

This project was financially supported by the CityU SRG Project #7002691.

References

1. S. Shabalovskaya, J. Cunnick, J. Anderegg, B. Harmon, and R. Sachdeva, Preliminary Data on in Vitro Study of Proliferative Rat Spleen Cell Response to Ni-Ti Surfaces Characterized Using ESCA Analysis, *Proceedings of the First International Conference on Shape Memory and Superelastic Technologies*, Vol. 209 (1994)
2. Y. Okazaki, Y. Ito, K. Kyo, and T. Tateishi, Corrosion Resistance and Corrosion Fatigue Strength of New Titanium Alloys for Medical Implants Without V and Al, *Mater. Sci. Eng., A*, 1996, **213**, p 138–147
3. H. Kawahara, A. Yamaguchi, and M. Nakamura, Biological Testing of Dental Materials by Means of Tissue Culture, *Int. Dent. J.*, 1968, **18**, p 443–467
4. S.G. Steinemann, Corrosion of Surgical Implants - In Vivo and In Vitro Tests, *Evaluation of Biomaterials*, G.D. Winter, J.L. Leray, and K. de Groot, Eds., John Wiley & Sons Ltd., New York, 1980, p 1–34

5. C. Baker, The Shape-Memory Effect in a Titanium-35 wt% Niobium Alloy, *Met. Sci. J.*, 1971, **5**, p 92–100
6. H.Y. Kim, H. Satoru, J.I. Kim, H. Hosoda, and S. Miyazaki, Mechanical Properties and Shape Memory Behavior of Ti-Nb Alloys, *Mater. Trans.*, 2004, **45**, p 2443–2448
7. J.I. Kim, H.Y. Kim, T. Inamura, H. Hosoda, and S. Miyazaki, Shape Memory Characteristics of Ti-22Nb-(2-8)Zr (at.%) Biomedical Alloys, *Mater. Sci. Eng., A*, 2005, **403**, p 334–339
8. S.H. Chang and S.K. Wu, Effect of Cooling Rate on Transformation Temperature Measurements of Ti50Ni50 Alloy by Differential Scanning Calorimetry and Dynamic Mechanical Analysis, *Mater. Charact.*, 2008, **59**, p 987–990
9. Q. Meng, H. Yang, Y. Liu, and T. Nam, Transformation Intervals and Elastic Strain Energies of B2-B19′ Martensitic Transformation of NiTi, *Intermetallics*, 2010, **18**, p 2431–2434
10. H.Y. Kim, J.I. Kim, T. Inamura, H. Hosoda, and S. Miyazaki, Effect of Thermo-Mechanical Treatment on Mechanical Properties and Shape Memory Behavior of Ti-(26-28) at.% Nb Alloys, *Mater. Sci. Eng., A*, 2006, **438–440**, p 839–843
11. D.J. Lin, J.H. Chern Lin, and C.P. Ju, Structure and Properties of Ti-7.5Mo-xFe Alloys, *Biomaterials*, 2002, **23**, p 1723–1730
12. P.J.S. Buenconsejo, H.Y. Kim, and S. Miyazaki, Effect of Ternary Alloying Elements on the Shape Memory Behavior of Ti-Ta Alloys, *Acta Mater.*, 2009, **57**, p 2509–2515